Ultramicroscopy 277 (2025) 114210

Contents lists available at ScienceDirect

Ultramicroscopy

journal homepage: www.elsevier.com/locate/ultramic

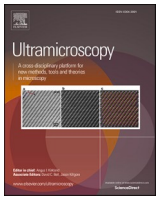

Cryogenic sample preparation: Comparative analysis of Ga^+ and Xe^+ FIB milling for TEM and APT examination of zirconium

Ömer Koç [a,*], Benjamin M. Jenkins [b,c,*], Jack Haley [b,d], Christina Hofer [b], Martin S. Meier [b], Megan E. Jones [b,e], Robert W. Harrison [a], Michael Preuss [a,f], Michael P. Moody [b], Christopher R.M. Grovenor [b], Philipp Frankel [a]

[a] Department of Materials, The University of Manchester, Oxford Road, M13 9PL, UK
[b] Department of Materials, University of Oxford, Parks Road, Oxford, OX1 3PH, UK
[c] University of Rouen Normandie, INSA Rouen Normandie, CNRS, Groupe de Physique des Matériaux UMR 6634, F-76000 Rouen, France
[d] UKAEA, Culham Science Centre, Abingdon, Oxfordshire OX14 3DB, UK
[e] National Nuclear Laboratory, Windscale Laboratory, Sellafield, Seascale, Cumbria CA20 1PG, United Kingdom
[f] Department of Materials Science and Engineering, Monash University, Clayton, VIC 3800, Australia

ARTICLE INFO

Keywords:
Cryo-FIB
Zirconium fuel cladding
Transmission electron microscopy (TEM)
Atom probe tomography (APT)
Hydrogen pick-up

ABSTRACT

Specimen preparation is a key step in the characterisation of materials systems. For high-resolution characterisation techniques such as transmission electron microscopy (TEM) and atom probe tomography (APT), it is necessary to have a sample preparation method that creates the nano-scale samples required for analysis but does not significantly modify the initial microstructure.

The preparation of hexagonal close-packed materials by focussed ion beam milling (FIB) and electropolishing has previously been shown to be complicated by hydride formation. The formation of hydrides can be reduced by the application of cryogenic temperatures during the final stages of Ga^+ ion FIB milling, which are often conducted at low accelerating voltages in order to minimise irradiation-induced damage.

Xe^+ ion plasma FIBs are now commonly used in the preparation of samples due to their higher milling rates. However, the severity of the hydride formation in hexagonal close-packed materials during Xe^+ ion milling is unclear. In this paper, we compare Xe^+ and Ga^+ FIB milling to prepare Zr samples at ambient and cryogenic temperatures. By studying TEM and APT samples, we are able to compare the levels of hydride formation after FIB preparation caused by the different preparation techniques. APT is used to estimate the levels of hydrogen in the samples. These results represent an important contribution to researchers who use FIB preparation to create TEM and APT specimens from hexagonal close-packed metals such as zirconium.

1. Introduction

Zirconium (Zr) alloys are widely utilised as structural materials in nuclear reactors. Light Water Reactor (LWR) fuel assemblies are subjected to extremely challenging conditions, including constant neutron flux and elevated temperatures, whilst also operating within a corrosive water environment. These harsh conditions cause damage to the Zr alloys' microstructure, degrading the properties of the alloy and restricting the service lifetime of Zr-based components inside the reactor [1].

Irradiation-induced changes in the microstructure, which are strongly correlated with the formation of dislocation loops, directly affect the mechanical properties by decreasing the ductility and also leading to irradiation-induced growth (IIG) [2,3]. IIG occurs due to the preferential formation of dislocation loops on various crystallographic planes, resulting from the anisotropy of the hexagonal closed-packed (HCP) structure [4,5], as well as the common split basal texture introduced by the manufacturing process [4]. This texture is a desired feature designed mainly to prevent radial crack propagation along hydrides that could align in this direction and can lead to failure [6]. However, hydride precipitation in zirconium claddings during nuclear reactor operation under irradiation is a significant cause of embrittlement, leading to the degradation of the mechanical properties of zirconium fuel cladding. Additionally, delayed hydride cracking (DHC) during storage is an important phenomenon related to the hydrogen pick up of

* Corresponding authors.
E-mail addresses: omerfkoc@gmail.com (Ö. Koç), ben.jenkins@ukaea.uk (B.M. Jenkins).

https://doi.org/10.1016/j.ultramic.2025.114210
Received 13 November 2024; Received in revised form 8 July 2025; Accepted 12 July 2025
Available online 13 July 2025

zirconium which requires attention [6,7]. The irradiation-induced dimensional instability observed in Zr fuel rods is also a limiting factor for reactor efficiency and safety. To generate a thorough understanding of the underlying mechanisms responsible for property changes during both service and long-term storage, it is essential to accurately characterise the evolution of microstructure, and particularly hydride nucleation and growth. This understanding will inform the design of better and safer fuel assemblies, which is expected to increase the reactor efficiency and safety and reduce the volume of radioactive waste.

Applying high-resolution characterisation techniques, such as transmission electron microscopy (TEM) and atom probe tomography (APT), to the study of radiation-induced microstructural changes is now a routine experimental process in many materials research facilities across the world. Both TEM and APT require specimens that have a thickness on the order of 100 nm or less and are produced via electropolishing and focused ion beam (FIB) milling. For some materials these preparation routes are known to cause changes in the materials, compromising our ability to observe the changes in materials' structures that arise during exposure to irradiation [8–10].

One specific challenge arises in the formation of hydrides in hexagonal close-packed (HCP) materials during their preparation for TEM and APT analysis. The formation of hydrides during sample preparation is especially unwanted since it not only changes the physical structure of the material, but it also severely limits our understanding of hydrogen-related phenomena, such as hydrogen embrittlement. Moreover, continuous irradiation can alter the morphology of hydrides, and potentially reduce their visibility due to interactions with irradiation introduced point defects which might trap hydrogen atoms reducing the size of the hydrides. Work by Hanlon et al. [8] and Mouton et al. [11] have shown that the use of cryogenic temperatures can mitigate this effect when preparing TEM and APT specimens from Zr samples with Ga^+ FIB. Mayweg et al. [12] observed similar behaviour, with a significant hydrogen content reduction after cryogenic temperature milling, although they report some level of hydrogen still exists in their APT specimens. Studies have demonstrated the same reduction in hydride formation and hydrogen introduction in Ti alloys prepared using cryo-FIB [13].

It should be noted that some level of hydrogen contamination is inevitable in APT due to the presence of hydrogen in the analysis chamber combined with the fact that the cold sample acts as a cryopump within the chamber. Nevertheless, APT is the only technique that is capable of providing local spatial hydrogen information on the scale of irradiation damage but distinguishing between real H in the sample and adventitious H from the experimental environment and from sample preparation routes is very challenging. The uncertainty in the source of the analysed hydrogen inhibits the ability of APT to confidently characterise hydrogen behaviour in Zr, which has therefore often necessitated the use of deuterium tracers [11,14]; one limitation of deuterium tracers is that they are often not present in-service specimens within nuclear power plants.

In addition to introducing hydrogen into specimens, another notable microstructural effect that is sometimes evident after FIB sample preparation is the introduction of point defects and dislocation loops due to ion beam damage. This effect is particularly significant when FIB milling is conducted at high accelerating voltages. There is, therefore, a need to perform the final FIB milling at low accelerating voltages, but this is known to induce undesired hydride formation in HCP materials if performed at ambient temperatures [15,16].

The recent development of Xe^+ plasma FIBs offer the potential to prepare samples much more efficiently owing to the faster milling rates of such instruments. However, the impact of plasma FIBs on hydride formation in HCP materials has not been fully explored. Chang et al. [13] investigated the effectiveness of cryo-temperature milling on titanium alloys using a Xe^+ plasma FIB, and reported significantly less hydride formation compared to ambient temperature milling. Another study by Xiangli et al. [16] compares Ga^+ and Xe^+ FIB milling on FCC aluminium alloys, highlighting the superior sample preparation quality achieved by Xe^+ ion beam. This superiority is evidenced by thinner amorphous layers and reduced redeposition. However, it's important to note that this study does not delve into the investigation of hydrogen ingress and hydride formation.

In this article, we prepared two types of Zr alloys for TEM and APT analysis. Each material was prepared using both Ga^+ and Xe^+ FIBs at ambient and cryogenic temperatures. This enables us to study the fraction of hydrides that form under each condition and enables the use of APT to estimate hydrogen levels in the Zr matrix after FIB preparation. We also investigate how the APT analysis conditions affect the apparent hydrogen concentrations in the data. Our results show that, as well as reducing the volume fraction of hydrides that form in TEM samples, use of cryogenic FIB (Ga^+ and Xe^+) greatly reduces the level of hydrogen that is detected in the α-Zr matrix by APT.

2. Materials and methods

2.1. Materials

This study focussed on two Zr-based alloys: Nb-containing low-Sn ZIRLO and Nb-free Zircaloy-2. The nominal compositions of these alloys are detailed in Table 1. The manufacturing processes and heat treatments applied to each alloy have been previously documented in [17].

Both alloys were neutron-irradiated at 320 ± 10 °C up to a fluence of 16.2×10^{25} n/m^2 in the BOR-60 reactor [2]. Samples irradiated to damage levels of 3 dpa and 27 dpa were investigated. In addition to these neutron-irradiated samples, Low-Sn ZIRLO and Zircaloy-2 samples proton-irradiated at the University of Manchester's Dalton Cumbrian Facility (DCF) at 320 ± 10 °C to 0.15 dpa (1.38×10^{22} p/m^2) nominal dose at 60 % Bragg peak depth (calculated by SRIM [18]) were also investigated.

2.2. Experimental methods

Conventional metallographic, APT and, TEM sample preparation procedures [19–22] were used throughout this work apart from the use of cryogenic temperatures for the milling of some samples. APT and TEM specimens were prepared from the BOR-60 neutron-irradiated samples in two stages using FIB milling. Initial milling and lift-outs were performed using Ga^+ FIB at ambient temperatures and 30 kV accelerating voltages using an FEI Helios NanoLab 600i Ga^+ ion FIB at the UKAEA Materials Research Facility (MRF). Half of these samples were then transferred to National Nuclear Laboratory Central Laboratory, where final sample thinning was conducted at cryogenic temperatures (−90 °C) on a similar FEI Helios NanoLab 600i. A final FIB cleaning/polishing stage, also performed at −90 °C and an accelerating voltage of 2 kV and beam current of 190 pA, was applied to the APT specimens. The control APT samples underwent the same FIB milling procedures at ambient temperatures at the MRF. TEM samples were prepared using a final accelerating voltage of 5 kV to thin the samples because thinning at 2 kV was previously observed to introduce more hydrides at ambient temperature [8]. One set of TEM samples was prepared at cryogenic temperatures and one set at ambient temperatures.

For the proton irradiated samples, an FEI Helios Xe^+ plasma FIB (pFIB) microscope with a Leica VCT 500 Cryo Stage using liquid nitrogen (−130 °C) was utilised for APT and TEM specimen preparation while initial lift out procedures were done at ambient temperature. Both

Table 1
Nominal composition (wt. %) of the Zr alloys analysed in this study.

Alloy	Nb	Sn	Fe	Ni	Cr	O	Zr
Zircaloy-2	0.00	1.35	0.17	0.07	0.104	0.12	Balance
Low Sn ZIRLO	0.95	0.66	0.12	0.004	0.01	0.12	Balance

TEM foils and APT lift outs were prepared from the plateau (15–20 μm) depth of the samples at which SRIM predicted dpa is ~0.15 dpa. This is to prevent large dpa variations throughout the analysis volumes and to maintain microstructural consistency. Most of the thinning process for TEM specimen preparation was conducted at 30 kV accelerating voltage with Xe^+ ions using beam currents of 0.23 nA and 74 pA. After achieving transparency at 10 kV electron beam imaging, a final cleaning step was conducted at 2 kV using 19 pA until transparency was achieved under 5 kV electron beam imaging. APT tip shaping was initially performed using a current of 0.23 nA at 30 kV with Xe^+ ions. Subsequently, final tip sharpening was achieved by employing a current of 74 pA at 30 kV with Xe^+. Upon reaching an approximate tip diameter of 100 nm, a final cleaning/polishing step was undertaken utilising 19 pA at 2 kV with Xe^+.

APT analyses were conducted on a reflectron-fitted Cameca LEAP 5000-XR at the University of Oxford Nuclear Materials Atom Probe (NuMAP) Facility. To investigate the effect of analysis conditions on detected hydrogen levels, samples were analysed at a variety of temperatures and in both laser and voltage mode; the analysis conditions for individual datasets will be specified in figure captions and in the text, where appropriate. Reconstructions and analyses were performed in IVAS 3.8.8 and AtomProbeLab v0.2.4 was used for compositional calculations [23,24].

A combination of TEM and STEM were used to examine the TEM foils using a JEOL ARM200F operating at 200 kV with a cold field emission source for the BOR-60 samples, whilst the proton-irradiated samples were imaged using a Thermo Scientific Talos F200X field-emission TEM operating at 200 kV with a field emission electron source (X-FEG). In STEM mode, samples were usually examined on the $<2\bar{1}\bar{1}0>$ zone axis to reveal the distribution of hydrides and irradiation damage-induced dislocation loops.

3. Results

3.1. Ga^+ FIB – TEM results

Use of the cryogenic FIB preparation led to a large reduction in the volume fraction of hydrides present in the TEM foils when compared to those produced at ambient temperatures (Fig. 1). This reduction supports the observations made be Hanlon et al. [8] and facilitated the characterization of irradiation-induced defects. Fig. 1 presents a typical post-irradiation microstructure, highlighting features such as <*a*>-dislocation loops and chemical segregation of alloying elements (Fe/Sn/Cr) together with native second-phase particles (SPPs).

Fig. 1c shows a typical micrograph of the <*a*>-component dislocation loops in Zircaloy-2 neutron-irradiated to 3.5 dpa. The loops are observed to align in rows, oriented normal to the <*c*>-direction, commonly referred to as "corduroy contrast" [25,26]. EDX and APT

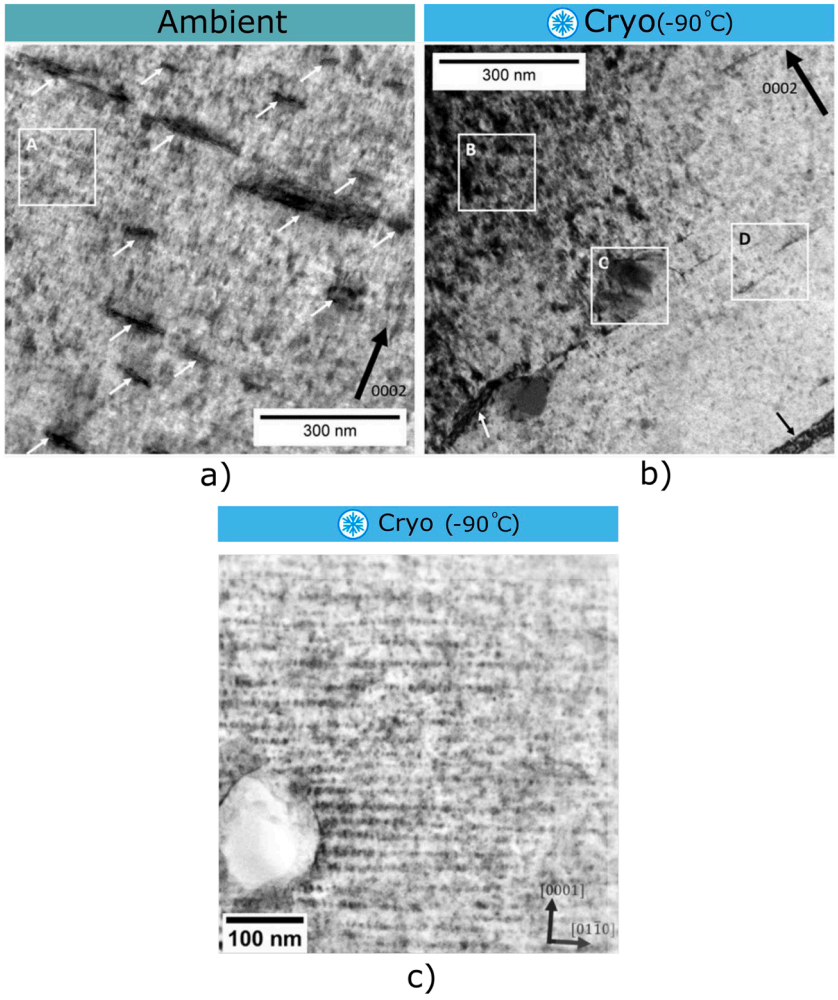

Fig. 1. A comparison of the microstructures of TEM foils of Zircaloy-2 neutron-irradiated to 3.5 dpa, prepared by FIB at ambient temperature (a) and - 90 °C (b). The imaging condition in a) and b) is a kinematical two-beam condition with $g = 0002$, close to $a < 2\bar{1}\bar{1}0>$ zone axis. Hydrides are indicated by small arrows. Other contrast in the images includes; (A, B) contrast from the chemical segregation around <*a*>-type loops (this is not visible in low-Sn ZIRLO); (*C) spps*; and (D) <*c*>-type dislocations. A typical STEM micrograph (c) depicting the microstructure captured with sample orientation close to the $<2\bar{1}\bar{1}0>$ zone axis.

analysis conducted previously has shown that similar rows of <*a*>-loops correlate strongly with the location of high Fe concentrations, and that the regions between the rows contain enhanced levels of Sn [17,27,28].

3.2. Xe^+ FIB – TEM results

Similar microstructure observations were made on the samples prepared with the use of cryogenic Xe^+ FIB. By cooling down the specimens to −130 °C during final FIB milling the prevention of almost any hydride formation in the TEM foils was achieved. This greatly enhances the ease and reliability of the analysis of irradiation damage when compared to samples prepared using ambient temperature FIB milling. Fig. 2 compares the FIB foils prepared at ambient temperature (a) and at −130 °C (b). Although Fig. 2(b) depicts a very clean region of the sample free from any hydrides, there were still some areas with hydrides present in very low volume fractions (Fig. 2(c)).

3.3. Ga^+ FIB – APT results

APT analyses were conducted to determine how much hydrogen was detected in both the cryo- and ambient-FIB samples after preparation. Analyses in both laser and voltage-pulsing modes were used to investigate whether analysis conditions affected the levels and distribution of hydrogen detected. The following hydrogen-containing ions were included in the peak overlap solving process: H^+, H_2^+, OH^+, H_2O^+, $ZrOH_2^{3+}$, ZrH^{2+}, ZrH_2^{2+}, ZrH^+ *and* ZrH_2^+. Fig. 3 demonstrates that performing the final APT sample shaping at cryogenic temperatures greatly reduces the levels of hydrogen detected in the analysed volume. A general observation was made that more hydrogen was detected in the ambient temperature FIB-prepared samples under analysis conditions which result in higher electrostatic fields (indicated by higher ratios of Zr^{3+}/Zr^{2+}), i.e. experiments conducted with lower laser energies or in voltage mode. Since some of the samples that were evaporated at the highest electrostatic fields contained large amounts of hydrogen (>40 at. %), we propose that these are likely to correspond to the hydride regions observed in TEM foils. This observation may indicate that $ZrH_{[x]}$ requires a higher electrostatic field for field evaporation than metallic Zr [29].

The use of cryo-FIB reduced the measured values of apparent matrix hydrogen levels to around 3 at. % in the atom probe samples, which is similar to levels reported in Ti alloys [13] and values reported by Mayweg et al. [12]. However, it is not possible to directly determine how representative this is of the true hydrogen levels in the original bulk material as opposed to how much arises from adventitious H introduced during analysis. This makes the quantification of the true hydrogen levels in α-Zr matrix difficult, although ways to estimate this have been

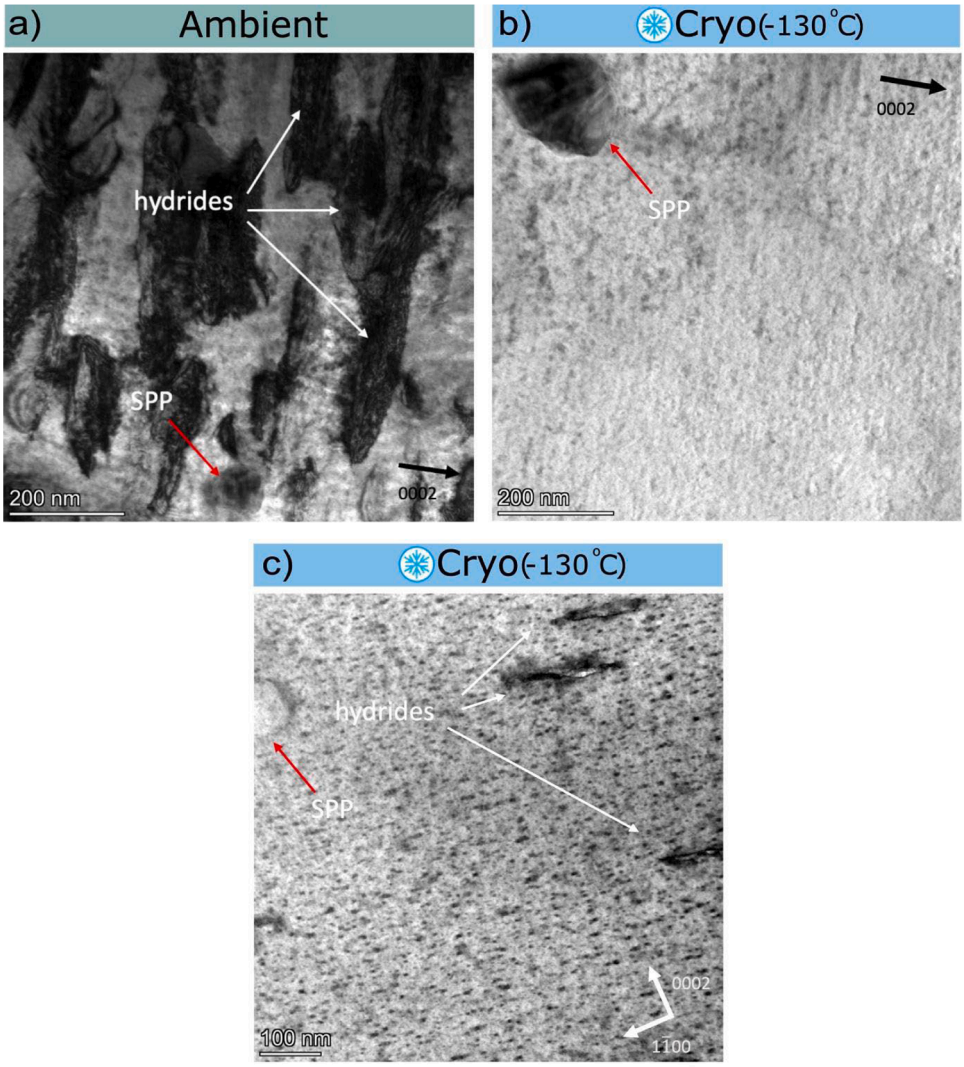

Fig. 2. A comparison of the microstructures of TEM foils of proton-irradiated Low-Sn ZIRLO irradiated to 0.15 dpa, prepared via FIB at ambient temperature (a)) and - 130 °C (b, c)). The imaging condition is a kinematical two-beam condition with $g = 0002$, close to $a < 2\bar{1}\bar{1}0>$ zone axis for a), b) and on zone axis $<2\bar{1}\bar{1}0>$ for c).

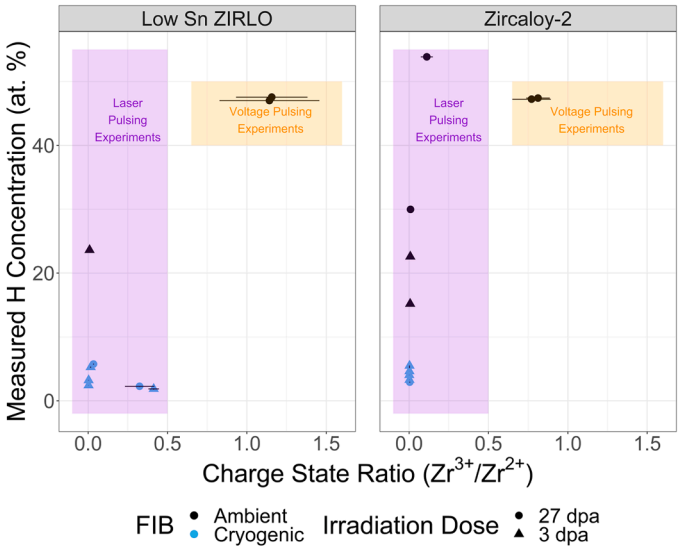

Fig. 3. Results comparing the levels of detected hydrogen in APT analysis in both of the Zr alloys prepared using FIB at ambient or cryogenic temperatures. The effect of field is also shown (as indicated by Zr^{3+}/Zr^{2+} ratio). A variety of laser energies (20 pJ - 80 pJ) were used as well as voltage-pulsing. Laser-pulsing was performed at 60 K and voltage-pulsing was performed at 70 K with a pulse fraction of 20 %.

recently proposed by Meier et al. [30]. They proposed that, under fixed analysis conditions, it can be expected for H present in the APT chamber to attach to the specimen at an approximately constant rate. Therefore, reducing the time between evaporation events of ions from the specimen will reduce the amount of time for H to absorb onto the surface and, as a result, less H will be detected during the experiment. Measuring H levels at several detection rates can be used to extrapolate to an effectively infinite evaporation rate (i.e. zero time for H from the chamber to absorb onto the sample), thus allowing an estimation of the true H content of the specimen. Applying this method to one dataset from Zircaloy-2 neutron-irradiated to 3 dpa, allows us to estimate the matrix hydrogen content in this sample to be 1.1 at. % (Fig. 4). This suggests that the samples do contain a non-zero level of bulk hydrogen after cryo-FIB preparation with Ga^+ FIB, but it is not possible to give an accurate quantitative value as to how much of this was present in the materials immediately after irradiation and how much was introduced during the cryo-FIB milling process. Since typical levels of hydrogen in neutron-irradiated Zr alloys are at least an order of magnitude lower [2,30,31], it is highly probable that a large fraction of hydrogen detected within the specimens is introduced during sample preparation, even at cryogenic temperatures, or during sample transfer.

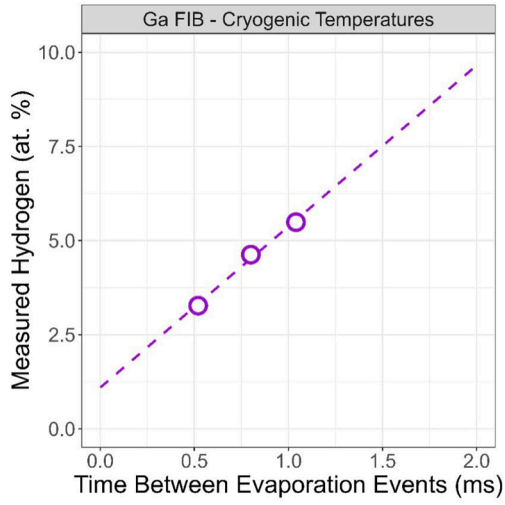

Fig. 4. Extrapolation of hydrogen fraction to zero time between evaporation events for a neutron-irradiated Zircaloy-2 to 3.5 dpa specimen prepared using Ga^+ FIB at cryogenic temperatures. Laser pulse energy was 80 pJ, detection rate was 1 %, and specimen temperature was 60 K.

The reduction of hydrogen introduced into the samples prepared at cryogenic temperatures compared to those prepared at ambient temperatures is advantageous since it will enhance the signal-to-noise ratio, where "signal" is defined as the hydrogenic species that arise from hydrogen that was present in the initial samples prior to FIB preparation and "noise" is any detected hydrogenic species from other sources. The datasets from samples prepared at cryogenic temperatures and analysed using voltage-pulsing or lower laser energies (20 pJ) had a random distribution of hydrogen ions (Fig. 5), as determined by comparing nearest neighbour distributions of hydrogen atoms with those in a mass-shuffled dataset [32]. This suggests that any hydrogen that is present in the α-Zr after irradiation or FIB milling is either homogeneously distributed or does not segregate strongly enough to microstructural features within the APT volumes to distinguish it from the background hydrogen that arises from the chamber during analysis.

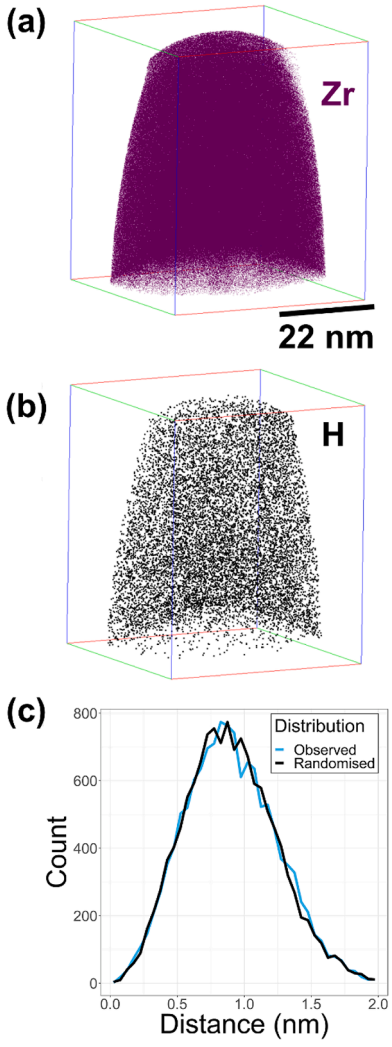

Fig. 5. Atom maps from cryo-FIBed sample showing (a) Zr and (b) hydrogen distributions in a low Sn ZIRLO sample irradiated to 27 dpa. (c) Shows the observed and mass-shuffled nearest neighbour distributions for H—H. This dataset contained 2.27 ± 0.09 at. % H. Analysis temperature = 60 K, laser pulse energy = 20 pJ. The bounding box for (a) and (b) is 45 nm x 46 nm x 55 nm.

However, using higher laser energies (80 pJ) did lead to a non-random distribution of hydrogen, with a higher concentration of hydrogen present on the side of the specimen opposite to the laser-incidence (Fig. 6). The non-randomness of the hydrogen distribution is clearly visible in the nearest neighbour distribution in Fig. 6(c).

The non-random distribution of hydrogen observed in Fig. 6 is likely an artefact due to the migration of H across the sample surface towards regions of high field [33]. At laser energies greater than 40 pJ, the hydrogen was consistently observed to be more concentrated on the non-laser-incident side of the atom probe samples, which is likely to complicate analyses of the spatial distribution of hydrogen in APT datasets.

3.4. Xe^+ FIB – APT results

A Zircaloy-2 specimen proton irradiated to 0.15 dpa at the Bragg peak was prepared with the same pFIB microscope used for TEM sample preparation utilising a Xe^+ plasma beam with the sample at ambient and cryogenic (−130 °C) temperatures. The APT data analysis procedure for estimating hydrogen content was conducted following the same methodology as employed for Ga^+ FIB prepared samples, including solving of overlapping peaks. When an extrapolation line is fitted to these data, as described by Meier et al. [30], the matrix hydrogen concentration is estimated to be 0.12 at. % in the proton irradiated Zircaloy-2 specimen (Fig. 7).

To compare the measured hydrogen content after Ga^+ FIB and Xe^+ FIB sample preparation, Fig. 8 presents the values obtained through APT analysis of samples prepared at both ambient and cryogenic temperatures. Both techniques yield comparable results, with much higher hydrogen content in samples prepared at ambient temperature; 50–55 at. % H and 3 – 5 at. % H respectively. This clearly shows the effectiveness of cryogenic sample preparation using both FIB ion beams. It can also be seen in Fig. 8 that there is one ambient temperature dataset containing very low hydrogen content from the Xe^+ FIB samples. The apparent deviation from the expected trend could be attributed to the possibility that this APT analysis examined a region free from preparation-induced hydrides. This observation is Fig. 2a, which illustrate that there are significant volumes of matrix material between the FIB-induced hydrides. This localized variation may account for the observed variance in the hydrogen content measurements in the samples prepared at ambient temperature.

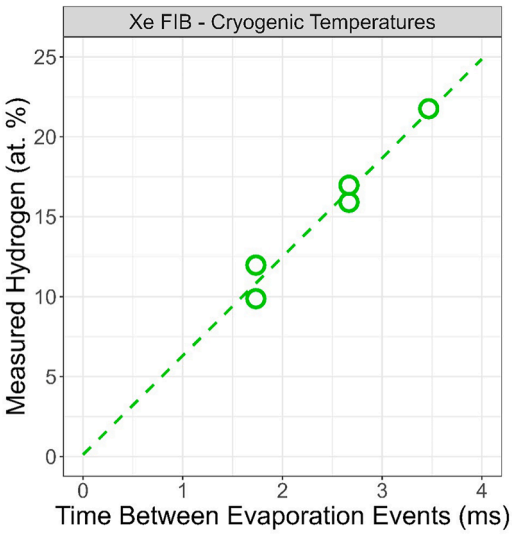

Fig. 7. Extrapolation of hydrogen fraction to zero time between evaporation events for Zircaloy-2 proton irradiated to 0.15 dpa. Laser pulse energy was 80 pJ, detection rate 0.3 %, and specimen temperature was 60 K.

4. Discussion

Care must be taken during FIB sample preparation if one wishes to quantitatively analyse an irradiated microstructure, especially in Zr-based alloys, due to the point defects and artefacts in the form of hydrides that are potentially introduced by the ion beams themselves. These features can obscure or complicate subsequent analyses of the original irradiation damage. Whilst it is assumed that the hydrogen content within the high vacuum environment of the FIB chamber, which can reach as low as 10^{-5} to 10^{-6} Pa depending on the equipment, is very low, this may not always be the case. For example, it has been repeatedly observed that even in APT systems, where the vacuum is much better (typically around 10^{-10} Pa), that the residual gas is mostly hydrogen [29, 34], and this can readily adsorb onto the surface of specimens. Performing the final FIB milling stages at cryogenic temperatures has been shown to greatly reduce the hydrogen introduced into both the TEM foils and APT samples of the Zr specimens studied here; this is beneficial as it allows quantitative analysis to be performed more easily on the original irradiated microstructure.

4.1. Cryogenic temperature prepared TEM foils

Cryogenic temperature thin foil preparation for TEM investigation proves advantageous for the analysis of irradiation-induced defects in HCP materials. This approach is particularly beneficial as it helps

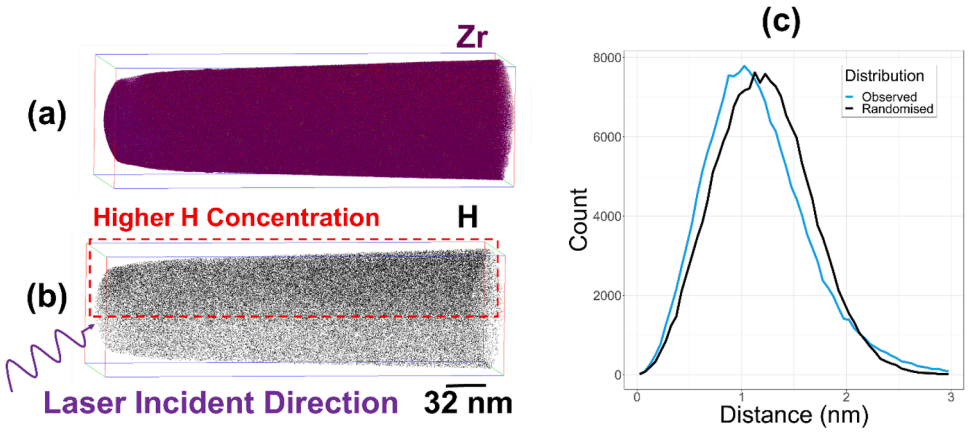

Fig. 6. Atom maps from cryo-FIBed sample showing (a) Zr and (b) hydrogen in low Sn ZIRLO sample irradiated to 27 dpa. (c) Shows the observed and mass-shuffled nearest neighbour distributions for H—H. Dataset contained 3.21 ± 0.02 at. % H. Analysis temperature = 60 K, laser pulse energy = 80 pJ. The bounding box in (a) and (b) is 96 nm x 100 nm x 323 nm.

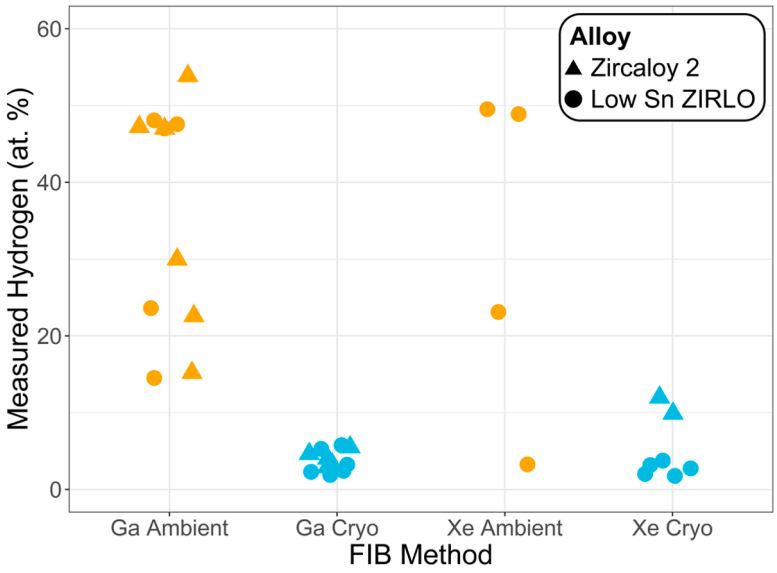

Fig. 8. APT measured hydrogen content (at. %) from Ga^+ FIB and Xe^+ FIB prepared samples at ambient and cryogenic temperatures. Specimens were analysed in both voltage and laser mode and using a variety of evaporation rates, which may explain some of the variance in the measured H level.

mitigate the risk of small hydrides being mistaken for dislocation loops, thereby improving the precision of quantifying defect concentrations. Furthermore, ambient-temperature prepared foils often show <*c*>-type dislocations near hydrides, thus posing the question as to whether the hydride nucleated at *a* < *c*>-dislocation, or the dislocation was formed due to the strain around the hydride when it nucleated [35]. The hydrides exert a large strain on the surrounding matrix due to the large lattice parameter mismatch [36], so there is a concern that significant FIB-induced hydriding could be causing unwanted changes to the microstructure. This includes potential changes in the nature of hydride formed in-service during subsequent ion beam milling at ambient temperature [2,11,12]. Thus, being able to minimise FIB-induced hydriding gives greater confidence in the microstructural characterisation.

Although both Ga^+ and Xe^+ plasma FIB milling methods induced hydride formation at ambient temperature, the extent was more pronounced after Xe^+ FIB milling (compare Figs. 1 and Fig. 2). The hydrides formed were longer (>~350 nm) for Xe^+ FIB versus (~200 nm) for Ga^+ FIB. This discrepancy could be caused by differences in the milling voltages employed for Ga^+ (5 kV) and Xe^+ (2 kV) milling at ambient temperature, as Hanlon et al. [8] showed that hydride formation is more pronounced at lower accelerating voltages. The observed differences in this study may also be influenced by factors such as the condition of the microscope, the runtime of the ion source (particularly if it is nearing servicing), residual chamber vacuum levels, and the milling current, which has been shown to affect hydride formation during milling [17]. Also, variations in time between sample preparation and analysis, during which the samples were left at ambient temperature, may impact the hydrogen levels in the samples. Additionally, the irradiation dose received by the samples prior to FIB preparation can impact the density of point defects and dislocations, thereby influencing hydride formation during sample preparation. Given the limited number of available TEM foils to enable an accurate and representative comparison between the two techniques, it is important to exercise caution in drawing definitive conclusions.

Additionally, it is worth noting that FIB milling itself might introduce radiation damage, which can influence hydrogen diffusivity, leading to its pickup and subsequent hydride formation [37,38]. However, this effect was found to be minimized by cryogenic temperature milling, which is believed to suppress point defect mobility, as demonstrated in a study by Li et al. [15] after their Ga^+ FIB milling experiments.

4.2. *Cryogenic temperature prepared APT tips*

After FIB milling at cryogenic temperatures, there were only small variations in the total levels of hydrogen detected during the APT experiments; this is likely because these experiments were all performed in laser mode with fairly similar times between evaporation events. In samples prepared at ambient temperatures, voltage-pulsing may lead to higher levels of hydrogen being detected during analysis when compared to samples analysed using high laser pulse energies. This observation aligns with [39], although Mayweg et al. [12] propose that voltage pulsing yields more consistent hydrogen content data compared to laser pulsing mode, based on their APT analysis of Zircaloy-2 specimens. However, Meier et al. [30] and this study have shown that the time between evaporation events is strongly correlated with measured hydrogen during APT experiments. Since the majority of articles in the literature fail to report this key parameter, it may be that some of the variations in measured hydrogen levels between laser and voltage mode is explained by the lower detection rates typically employed in voltage-pulsing experiments, which leads to an increase in time between evaporation events.

4.3. *Comparisons between Ga^+ vs Xe^+ FIB*

When comparing Ga^+ and Xe^+ FIB milled samples, a similar reduction in hydrogen content was observed after cryogenic temperature milling (Fig. 8) which might be aided by the low diffusivity of hydrogen at this temperature [13,15]. Extrapolation to higher evaporation rates allows us to estimate the initial bulk hydrogen content of the samples prior to APT analysis [30], which might also be affected by the irradiation dose and hence the dislocation density of the starting material.

Fig. 9 depicts the hydrogen content measured after employing varying pulse frequencies on both Ga^+ FIB and Xe^+ FIB prepared samples. As expected, both samples have decreasing measured hydrogen content as the time between evaporation events decreases. Extrapolation to zero time between evaporation events indicates that the cryogenic Xe^+ FIB sample appears to have a slightly lower hydrogen content (0.1 ± 5.4 at. % vs 1.1 ± 3.7 at. % for the Ga^+ FIB sample), although the 95 % confidence intervals for the two fits overlap. It is therefore not possible to definitively determine if there is a difference in the level of hydrogen introduced by Xe^+ and Ga^+ ion beams. Potential differences might be attributed to the difference in ion weight resulting in a higher sputtering

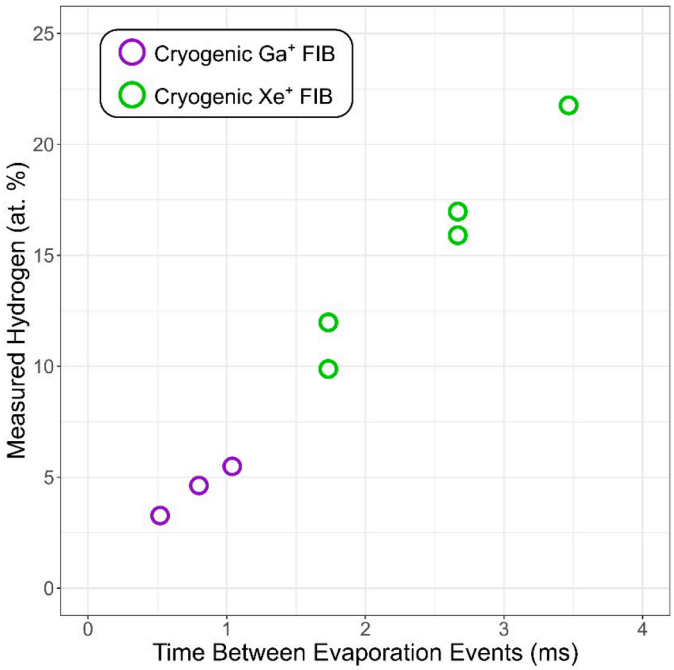

Fig. 9. The hydrogen analysis results obtained from APT for tips prepared using both Ga^+ FIB (Zircaloy-2 to 3.5 dpa) and Xe^+ FIB (Zircaloy-2 to 0.15 dpa) methods were overlaid in the same plot, revealing similar trends. Both experiments were performed at 60 K using a laser pulse energy of 80 pJ.

rate for the Xe^+ FIB [16], implying that Xe^+ ions induce less damage to the material below the surface [40,41] and potentially less implantation of hydrogen into the bulk of the material. This could lead to hydrogen being confined mostly at the near surface of the material and might account for the observed lower bulk hydrogen content after Xe^+ FIB preparation (Fig. 7). Another possible source of the difference is that the Xe^+ cryo-FIB preparation was performed at a slightly lower temperature (−130 °C) than the Ga^+ cryo-FIB (−90 °C), which may impact the diffusion rate of hydrogen into the samples during FIB milling. However, caution should be exercised in attributing this difference solely to the different temperatures since there are other potential explanatory variables, such as the residual hydrogen content of the chambers of the different FIB instruments, that are unknown and may vary appreciably. As a result, we suggest that the different intercepts at 0.1 at. % and 1.1 at. % in the cryo-FIB experiments do not yet give us confidence that use of the Xe^+ ion FIB is introducing less H into the samples than the Ga^+ ion FIB.

The APT-estimated level of 0.1 at % H content in proton-irradiated Zircaloy-2 after FIB preparation is consistent with the SRIM calculations, see Fig. 10. The value calculated by SRIM is below 0.1 at % H at the plateau depth of proton irradiation where the APT investigations were performed. This finding shows that the SRIM hydrogen implantation calculation matches the measured values fairly well.

5. Summary and conclusions

The interaction of hydrogen atoms with zirconium alloys is of high interest to the nuclear materials community. However, experimentally imaging hydrogen is difficult and further complicated by the fact the standard sample preparation methods can induce hydride formation in specimens. This also impacts the ease and reliability with which irradiation-induced damage in zirconium alloys can be characterised.

In this article both cryogenic Ga^+ and Xe^+ ion beam-prepared specimens demonstrated a notable decrease in hydride formation and a reduced introduction of hydrogen compared to the same methods performed at ambient temperatures. The bulk hydrogen content per sample before APT analysis was found to be lower in cryo Xe^+ prepared samples compared to cryo Ga^+ prepared ones. This difference may be attributed to the lower implantation depth of Xe^+ ions, differences in the FIB instruments (e.g. stage temperature, hydrogen content of the FIB chamber) that were used, or it may be because of pick-up during sample preparation and different irradiation exposure conditions of the samples that were analysed leading to differing levels of hydrogen within the specimens prior to FIB preparation. Indeed, the limited number of samples analysed in this study underscores the need for further investigation into the topic, but it appears that zirconium specimens prepared

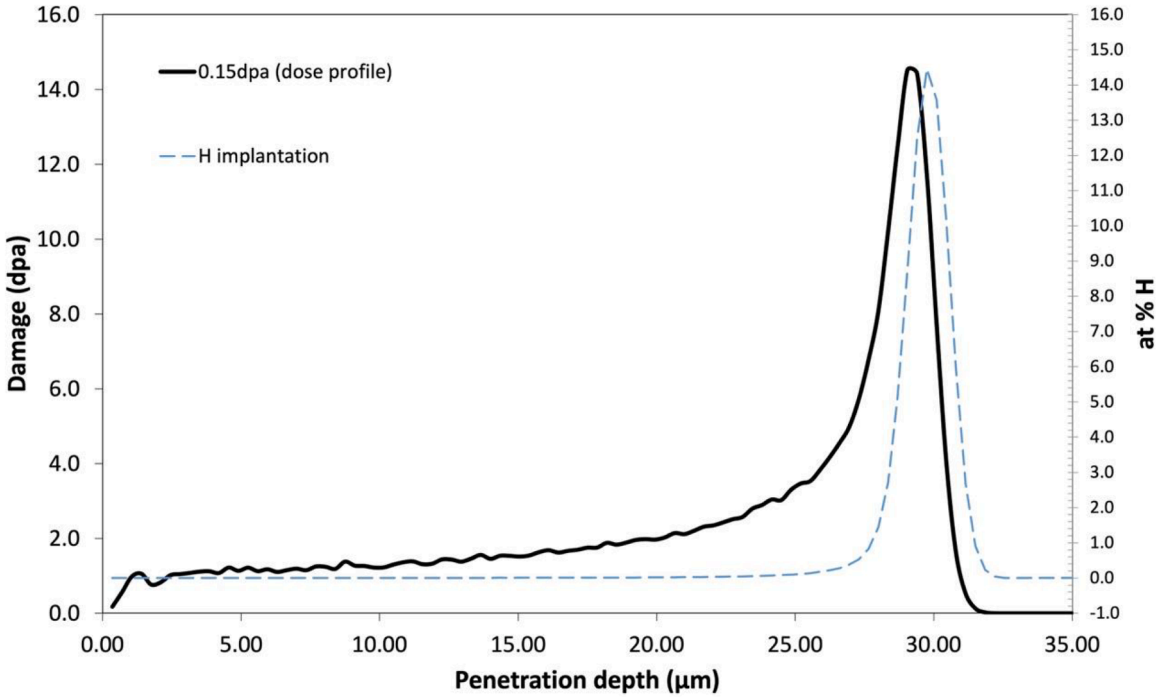

Fig. 10. SRIM calculated damage and hydrogen implantation profile of a 0.15 dpa (60 % Bragg peak) proton irradiated Zr.

using Xe^+ ions at cryogenic temperatures are comparable to those prepared using Ga^+ ions under the same conditions.

The consistent maintenance of cryogenic temperatures by the cryo-stage during the final sharpening/thinning procedure is crucial for minimising any hydrogen uptake by the Zr alloys. Therefore, cryo-FIB should be used whenever possible to enhance the reliability of TEM and APT data. Future work should investigate the role of transferring samples under vacuum and cryogenic temperatures between the FIB and TEM/APT to study the influence that this may have on measured hydrogen levels. Once these issues are addressed, it may be possible to organise systematic studies that investigate the relationship between irradiation damage, hydrogen trapping, and hydride formation.

CRediT authorship contribution statement

Ömer Koç: Writing – original draft, Methodology, Investigation, Formal analysis, Conceptualization. **Benjamin M. Jenkins:** Writing – review & editing, Writing – original draft, Visualization, Methodology, Investigation, Formal analysis, Data curation, Conceptualization. **Jack Haley:** Writing – review & editing, Investigation, Data curation. **Christina Hofer:** Writing – review & editing, Software, Formal analysis, Data curation. **Martin S. Meier:** Writing – review & editing, Investigation, Formal analysis, Conceptualization. **Megan E. Jones:** Writing – review & editing, Formal analysis, Conceptualization. **Robert W. Harrison:** Writing – review & editing, Supervision, Investigation, Formal analysis, Conceptualization. **Michael Preuss:** Writing – review & editing, Supervision, Investigation, Funding acquisition, Formal analysis, Conceptualization. **Michael P. Moody:** Writing – review & editing, Supervision, Project administration, Investigation, Conceptualization. **Christopher R.M. Grovenor:** Writing – review & editing, Writing – original draft, Project administration, Investigation, Funding acquisition, Formal analysis, Conceptualization. **Philipp Frankel:** Writing – review & editing, Writing – original draft, Supervision, Project administration, Funding acquisition, Formal analysis, Data curation, Conceptualization.

Declaration of competing interest

The authors declare that they have no known competing financial interests or personal relationships that could have appeared to influence the work reported in this paper.

Acknowledgements

The atom probe facilities at the University of Oxford are funded by the Engineering and Physical Sciences Research Council (EPSRC) grants EP/M022803/1 and EP/T011505/1. The research used UKAEA's Materials Research Facility, which has been funded by and is part of the UK's National Nuclear User Facility and Henry Royce Institute for Advanced Materials (EP/R00661X/1). The authors would like to acknowledge funding from EPSRC program grant MIDAS (EP/S01702X/1) for the study of irradiation damage in zirconium alloys. This research was part funded under the £46 m Advanced Fuel Cycle Programme (AFCP) as part of the Department for Business, Energy and Industrial Strategy's (BEIS) £505 m Energy Innovation Programme and the TEM at National Nuclear Laboratory was funded by EPSRC grant EP/I034106/1. ÖK would like to acknowledge funding by Republic of Türkiye, Ministry of National Education. BMJ is a recipient of the WINNING-Normandy Program the Normandy Region and would like to acknowledge this project has received funding from the European Union's Horizon 2020 research and innovation programme under the Marie Sklodowska Curie grant agreement No. 101034329. MEJ would like to acknowledge funding by EPSRC, National Nuclear Laboratory and Rolls-Royce plc. MSM would like to acknowledge funding from Cameca Instruments Inc / AMETEK Inc, USA

Data availability

Data will be made available on request.

References

[1] F. Onimus, S. Doriot, J.L. Béchade, Radiation Effects in Zirconium Alloys, 2020. https://doi.org/10.1016/B978-0-12-803581-8.11759-X.
[2] S. Yagnik, R. Adamson, G. Kobylyansky, J.-H. Chen, D. Gilbon, S. Ishimoto, T. Fukuda, L. Hallstadius, A. Obukhov, S. Mahmood, Effect of alloying elements, cold work, and hydrogen on the irradiation-induced growth behavior of zirconium alloy variants, Zircon. Nucl. Ind. 18th Int. Symp. (2018) 748–795, https://doi.org/10.1520/stp159720160040.
[3] N. Industry, Irradiation Growtii of Zircaloy, (2020) 326–343.
[4] E. Tenckhoff, Review of deformation mechanisms, texture, and mechanical anisotropy in zirconium and zirconium base alloys, Zircon. Nucl. Ind. Fourteenth Int. Symp. 2 (2008) 25–26, https://doi.org/10.1520/stp37501s, 25-.
[5] R.B. Adamson, C.E. Coleman, M. Griffiths, Irradiation creep and growth of zirconium alloys: a critical review, J. Nucl. Mater. 521 (2019) 167–244, https://doi.org/10.1016/j.jnucmat.2019.04.021.
[6] A.T. Motta, L. Capolungo, L.Q. Chen, M.N. Cinbiz, M.R. Daymond, D.A. Koss, E. Lacroix, G. Pastore, P.C.A. Simon, M.R. Tonks, B.D. Wirth, M.A. Zikry, Hydrogen in zirconium alloys: a review, J. Nucl. Mater. 518 (2019) 440–460, https://doi.org/10.1016/j.jnucmat.2019.02.042.
[7] J. Bair, M. Asle Zaeem, M. Tonks, A review on hydride precipitation in zirconium alloys, J. Nucl. Mater. 466 (2015) 12–20, https://doi.org/10.1016/j.jnucmat.2015.07.014.
[8] S.M. Hanlon, S.Y. Persaud, F. Long, A. Korinek, M.R. Daymond, A solution to FIB induced artefact hydrides in Zr alloys, J. Nucl. Mater. 515 (2019) 122–134, https://doi.org/10.1016/j.jnucmat.2018.12.020.
[9] A.T.W. Barrow, A. Korinek, M.R. Daymond, Evaluating zirconium-zirconium hydride interfacial strains by nano-beam electron diffraction, J. Nucl. Mater. 432 (2013) 366–370, https://doi.org/10.1016/j.jnucmat.2012.08.003.
[10] Z. Yang, F. Li, J. Yao, S. Li, Y. Wang, The HRTEM characterization of electropolishing-induced ζ-hydride in the α-Zr/δ-hydride interface in Zircaloy-4, Mater. Lett. 335 (2023) 133713, https://doi.org/10.1016/j.matlet.2022.133713.
[11] I. Mouton, Y. Chang, P. Chakraborty, S. Wang, L.T. Stephenson, T. Ben Britton, B. Gault, Hydride growth mechanism in zircaloy-4: investigation of the partitioning of alloying elements, Materialia 15 (2021) 101006, https://doi.org/10.1016/j.mtla.2021.101006.
[12] D. Mayweg, J. Eriksson, O. Bäcke, A.J. Breen, M. Thuvander, Focused Ion Beam induced hydride formation does not affect Fe, Ni, Cr-clusters in irradiated Zircaloy-2, J. Nucl. Mater. 581 (2023) 154444, https://doi.org/10.1016/j.jnucmat.2023.154444.
[13] Y. Chang, W. Lu, J. Guénolé, L.T. Stephenson, A. Szczpaniak, P. Kontis, A. K. Ackerman, F.F. Dear, I. Mouton, X. Zhong, S. Zhang, D. Dye, C.H. Liebscher, D. Ponge, S. Korte-Kerzel, D. Raabe, B. Gault, Ti and its alloys as examples of cryogenic focused ion beam milling of environmentally-sensitive materials, Nat. Commun. 10 (2019), https://doi.org/10.1038/s41467-019-08752-7.
[14] I. Mouton, A.J. Breen, S. Wang, Y. Chang, A. Szczepaniak, P. Kontis, L. T. Stephenson, D. Raabe, M. Herbig, T. Ben Britton, B. Gault, Quantification challenges for atom probe tomography of hydrogen and deuterium in Zircaloy-4, Microsc. Microanal 25 (2019) 481–488, https://doi.org/10.1017/S143192761801615X.
[15] F. Li, S. Li, Y. Wang, TEM-studies of the element segregation in irradiation induced defect structure in Zircaloy-4, Vacuum 200 (2022) 111053, https://doi.org/10.1016/j.vacuum.2022.111053.
[16] X. Zhong, C.A. Wade, P.J. Withers, X. Zhou, C. Cai, S.J. Haigh, M.G. Burke, Comparing Xe+pFIB and Ga+FIB for TEM sample preparation of Al alloys: minimising FIB-induced artefacts, J. Microsc. 282 (2021) 101–112, https://doi.org/10.1111/jmi.12983.
[17] B.M. Jenkins, J. Haley, M.P. Moody, J.M. Hyde, C.R.M. Grovenor, APT and TEM study of behaviour of alloying elements in neutron-irradiated zirconium-based alloys, Scr. Mater. 208 (2022) 114323, https://doi.org/10.1016/j.scriptamat.2021.114323.
[18] R.E. Stoller, M.B. Toloczko, G.S. Was, A.G. Certain, S. Dwaraknath, F.A. Garner, Erratum: (On the use of SRIM for computing radiation damage exposure (2013) 310 (75–80), (S0168583X13005053), (10.1016/j.nimb.2013.05.008)), Nucl. Instruments Methods Phys. Res. Sect. B Beam Interact. with Mater. Atoms. 459 (2019) 196–197, https://doi.org/10.1016/j.nimb.2019.08.015.
[19] K. Thompson, D. Lawrence, D.J. Larson, J.D. Olson, T.F. Kelly, B. Gorman, In situ site-specific specimen preparation for atom probe tomography, Ultramicroscopy 107 (2007) 131–139, https://doi.org/10.1016/j.ultramic.2006.06.008.
[20] M.K. Miller, K.F. Russell, G.B. Thompson, Strategies for fabricating atom probe specimens with a dual beam FIB, Ultramicroscopy 102 (2005) 287–298, https://doi.org/10.1016/j.ultramic.2004.10.011.
[21] G. Ashiotis, A. Deschildre, Z. Nawaz, J.P. Wright, D. Karkoulis, F.E. Picca, J. Kieffer, The fast azimuthal integration Python library: pyFAI, J. Appl. Crystallogr. 48 (2015) 510–519, https://doi.org/10.1107/S1600576715004306.
[22] Ö. Koc, R. Thomas, X. Liang, Z. Hegedues, U. Lienert, R.W. Harrison, M. Preuss, T. Ungar, P. Frankel, A spatially resolved analysis of dislocation loop and nanohardness evolution in proton irradiated zircaloys, Acta Mater. (2024), https://doi.org/10.1016/j.actamat.2024.119799.

[23] A.J. London, Quantifying uncertainty from mass-peak overlaps in atom probe microscopy, Microsc. Microanal. 25 (2019) 378–388, https://doi.org/10.1017/S1431927618016276.
[24] A.J. London, Atom Probe Lab (2019). https://sourceforge.net/projects/atomprobelab/.
[25] D.O. Northwood, R.W. Gilbert, L.E. Bahen, P.M. Kelly, R.G. Blake, A. Jostsons, P. K. Madden, D. Faulkner, W. Bell, R.B. Adamson, Characterization of neutron irradiation damage in zirconium alloys - an international "round-robin" experiment, J. Nucl. Mater. 79 (1979) 379–394, https://doi.org/10.1016/0022-3115(79)90103-X.
[26] A. Harte, D. Jädernäs, M. Topping, P. Frankel, C.P. Race, J. Romero, L. Hallstadius, E.C. Darby, M. Preuss, The effect of matrix chemistry on dislocation evolution in an irradiated Zr alloy, Acta Mater. (2017), https://doi.org/10.1016/j.actamat.2017.03.024.
[27] G. Sundell, M. Thuvander, P. Tejland, M. Dahlbäck, L. Hallstadius, H.O. Andrén, Redistribution of alloying elements in Zircaloy-2 after in-reactor exposure, J. Nucl. Mater. 454 (2014) 178–185, https://doi.org/10.1016/j.jnucmat.2014.07.072.
[28] A. Harte, M. Topping, P. Frankel, D. Jädernäs, J. Romero, L. Hallstadius, E. C. Darby, M. Preuss, Nano-scale chemical evolution in a proton-and neutron-irradiated Zr alloy, J. Nucl. Mater. 487 (2017) 30–42, https://doi.org/10.1016/j.jnucmat.2017.01.049.
[29] S.H. Yoo, S.H. Kim, E. Woods, B. Gault, M. Todorova, J. Neugebauer, Origins of the hydrogen signal in atom probe tomography: case studies of alkali and noble metals, New J. Phys. 24 (2022) 013008, https://doi.org/10.1088/1367-2630/ac40cd.
[30] M.S. Meier, M.E. Jones, P.J. Felfer, M.P. Moody, D. Haley, Extending estimating hydrogen content in atom probe tomography experiments where H 2 molecule formation occurs, Microsc. Microanal. 28 (2022) 1231–1244, https://doi.org/10.1017/S1431927621012332.
[31] A.T. Motta, A. Couet, R.J. Comstock, Corrosion of zirconium alloys used for nuclear fuel cladding, Annu. Rev. Mater. Res. 45 (2015) 311–343, https://doi.org/10.1146/annurev-matsci-070214-020951.
[32] T. Philippe, O. Cojocaru-MirÉdin, S. Duguay, D. Blavette, Clustering and nearest neighbour distances in atom probe tomography: the influence of the interfaces, J. Microsc. 239 (2010) 72–77, https://doi.org/10.1111/j.1365-2818.2009.03359.x.
[33] T.T. Tsong, G. Kellogg, Direct observation of the directional walk of single adatoms and the adatom polarizability, Phys. Rev. B. 12 (1975) 1343–1353, https://doi.org/10.1103/PhysRevB.12.1343.
[34] P. Felfer, B. Ott, M. Monajem, V. Dalbauer, M. Heller, J. Josten, C. MacAulay, An atom probe with ultra-low hydrogen background, Microsc. Microanal. 28 (2022) 1255–1263, https://doi.org/10.1017/S1431927621013702.
[35] L. Tournadre, F. Onimus, J.L. Béchade, D. Gilbon, J.M. Cloué, J.P. Mardon, X. Feaugas, Toward a better understanding of the hydrogen impact on the radiation induced growth of zirconium alloys, J. Nucl. Mater. 441 (2013) 222–231, https://doi.org/10.1016/j.jnucmat.2013.05.045.
[36] E.A. Gulbransen, K.F. Andrew, Crystal structure and thermodynamic studies on the zirconium-hydrogen alloys, J. Electrochem. Soc. 101 (1954) 474, https://doi.org/10.1149/1.2781303.
[37] M. Sugiyama, G. Sigesato, A review of focused ion beam technology and its applications in transmission electron microscopy, J. Electron Microsc. (Tokyo). 53 (2004) 527–536, https://doi.org/10.1093/jmicro/dfh071.
[38] B.M. Jenkins, J.O. Douglas, N. Almirall, N. Riddle, P.A.J. Bagot, J.M. Hyde, G. R. Odette, M.P. Moody, The effect of composition variations on the response of steels subjected to high fluence neutron irradiation, Materialia 11 (2020) 100717, https://doi.org/10.1016/j.mtla.2020.100717.
[39] G. Sundell, M. Thuvander, H.O. Andrén, Hydrogen analysis in APT: methods to control adsorption and dissociation of H2, Ultramicroscopy 132 (2013) 285–289, https://doi.org/10.1016/j.ultramic.2013.01.007.
[40] R.D. Kelley, K. Song, B. Van Leer, D. Wall, L. Kwakman, Xe+ FIB milling and measurement of amorphous silicon damage, Microsc. Microanal. 19 (2013) 862–863, https://doi.org/10.1017/s1431927613006302.
[41] K. Eder, V. Bhatia, J. Qu, B. Van Leer, M. Dutka, J.M. Cairney, A multi-ion plasma FIB study: determining ion implantation depths of Xe, N, O and Ar in tungsten via atom probe tomography, Ultramicroscopy 228 (2021) 113334, https://doi.org/10.1016/j.ultramic.2021.113334.